THE JOURNAL OF PHYSICAL CHEMISTRY B

Article

pubs.acs.org/JPCB

Fractional Crystallization and Homogeneous Nucleation of Confined PEG Microdomains in PBS-PEG Multiblock Copolymers

Cai-Li Huang, Ling Jiao, Jian-Bing Zeng, Jing-Jing Zhang, Ke-Ke Yang,* and Yu-Zhong Wang*

Center for Degradable and Flame-Retardant Polymeric Materials (ERCPM-MoE), College of Chemistry, State Key Laboratory of Polymer Materials Engineering, National Engineering Laboratory of Eco-Friendly Polymeric Materials (Sichuan), Sichuan University, 29 Wangjiang Road, Chengdu 610064, China

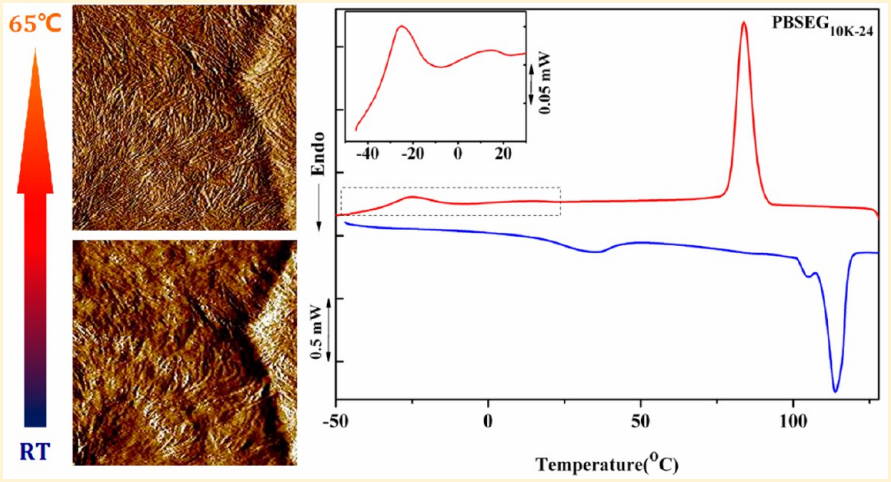

ABSTRACT: Fractional crystallization, homogeneous nucleation of poly(ethylene glycol) (PEG) segment, and self-nucleation behavior of PEG segment within miscible double crystalline poly(butylene succinate)-poly(ethylene glycol) (PBSEG) multiblock copolymers with different composition and segment chain length were studied by differential scanning calorimetry (DSC). Surface morphology of $PBSEG_{10K}$ with different PEG content was investigated by atomic force microscope (AFM). Different from di- or triblock copolymers, the microstructure and confinement of PEG dispersed phase in PBS matrix phase highly depends on chain length and sequence as well as segment content. The transition point of the PEG segment content from heterogeneous to homogeneous nucleation mechanism decreased from 50 to 39 wt % with PEG segment chain length increasing from 1000 to 2000 g/mol. When PEG segment chain length increased further to 6000 and 10000 g/mol, homogeneous nucleation phenomenon took place at much lower PEG content and fractional crystallization was observed at 29 and 24 wt %, respectively. Homogeneous nucleation mechanism of $PBSEG_{1K-36}$, $PBSEG_{2K-26}$, $PBSEG_{6K-19}$, and $PBSEG_{10K-12}$ was evidenced by the large supercoolings needed for crystallization, as well as first-order crystallization kinetics obtained. Self-nucleation behaviors of PEG segment still rely on the composition of PBSEGs. In the case of heterogeneous nucleation crystallization, self-nucleation behaviors of PEG segment showed standard self-nucleation behavior with classical three self-nucleation domains. When the crystallizable chains were confined into isolated microdomains, however, self-nucleation domain (domain II) disappeared. The absence of III_A was observed in $PBSEG_{2K-39}$, while $PBSEG_{6K-29}$ had both III_A and III_{SA}. Furthermore, AFM morphology studies still indicated the confined degree of PEG segment by previous PBS crystals was profoundly influenced by segment fraction. The confinement of the PEG segment by previous PBS edge-on lamellae was observed in the sample which displays a homogeneous nucleation crystallization behavior.

INTRODUCTION

The crystallization behaviors of semicrystalline polymers has attracted more and more attentions from both academic and industrial fields, since they profoundly affect the physical properties of polymers.[1−13] Compared to the homopolymer, the crystallization behaviors of multicomponent polymers, such as block copolymers or blends, are much more complex. The early research works used to focus on block copolymers with only one crystalline block,[13−17] and some mutual theories were well established.

Recently, double crystalline multicomponent copolymers, especially double crystalline di- or triblock copolymers, are of great attraction and highly investigated.[18−22] In the case of double crystalline block copolymers, the second segment could be confined within preformed lamellar stacks microdomain of the first segment, or nucleated by preformed crystal of the first

Received: June 17, 2013
Revised: August 13, 2013
Published: August 16, 2013

dx.doi.org/10.1021/jp4059966 | J. Phys. Chem. B 2013, 117, 10665−10676

segment. Confined crystallization can lead to fractional crystallization. Fractional crystallization phenomenon occurs due to the crystallizations of a series of domains at specific and independent supercoolings.[23] Domains with different numbers of heterogeneities induce various degrees of nucleation effect, some of which even do not contain any heterogeneity, and thus polymer chains or segments could crystallize at different temperatures.[23] In the case of fractional crystallization, one of the components is able to crystallize at much higher temperature than the other component. When the crystallization of the first component occurs, the second component remains in melt. With the sample further cooled, the second component crystallizes in a confined way within the interlamellar regions of the first component.[24] This phenomenon can be found in many situations, such as droplet suspension,[25,26] immiscible polymer blends,[23,26−32] or block copolymers.[33−39] For polymer blends and block copolymers, fractional crystallization generally takes place in immiscible systems. Recently, fractional crystallization has also been found in miscible systems. He et al.[24] first reported fractionated crystallization and homogeneous nucleation crystallization of poly(ethylene oxide) (PEO). Similarly, fractional crystallization phenomenon in miscible PEO/poly(hydroxybutyrate) (PHB) blends[40] and poly(butylene adipate) (PBA)/poly(vinylidene fluoride) (PVDF) blends[41,42] has been reported. Additionally, fractional crystallization and homogeneous nucleation of PCL segment in miscible PEG-PCL[43] and PLLA-PCL[44] diblock copolymers were found. Nevertheless, most investigations are focused on blends or dibock copolymers, fractional crystallization and homogeneous nucleation in miscible multiblock copolymers are seldom involved. In a multiblock copolymer, each polymer segment is spaced by the other segments into short pieces, and the chain irregularity is seriously disturbed especially in the copolymer with very short segment chain length. Thus, the double crystalline multiblock copolymers will exhibit more intricate crystallization behavior. Naturally, the sequence distribution and chain length of the copolymer segments will play important roles as well as their content. So it is very necessary to explore the fractional crystallization behaviors of low-T_m segment in the multiblock copolymers system.

In our previous works, we have prepared PBSEG multiblock copolymers with good shape memory effect,[45] and studied crystallization kinetics and morphology of the double crystalline PBSEG multiblock copolymers.[46] In the present paper, we address fractional crystallization behavior and nucleation mechanism of PEG segment within PBSEG. This investigation can be a guidance for understanding how these crystallization properties change in miscible multblock copolymers.

EXPERIMENTAL SECTION

Synthesis. PBSEGs were synthesized by a two-step transesterification reaction in bulk. Detailed procedures were previously reported.[45] The products were purified by dissolving in chloroform and then precipitating in excess of ether. The white powder products were dried to constant weight in vacuum condition. In order to investigate the influence of structure and composition of multiblock copolymer on the fractional crystallization behavior, a series of PBSEG with different PEG chain segment lengths and contents were prepared by varying the molecular weight of PEG diol and feed ratio (Table 1). All multiblock copolymer samples were recorded as PBSEG$_{xK\text{-}y}$, where "x" refers to the molecular weight of PEG diol (10^3 g/mol), and "y" refers to the weight fraction of PEG segment (F_{PEG}) within multiblock copolymers (calculated by ^{1}H NMR spectra). For example, PBSEG$_{2K\text{-}29}$ means that the molecular weight of PEG diol is 2000 g/mol, and the weight fraction of PEG segment is 29 wt % in the resultant PBSEG. The molecular weight of PBSEGs was determined by gel permeation chromatography (GPC).

Table 1. Designation, Composition, and Molecular Weight of PBSEGs

sample	$M_{n,PEG}$ (10^3 g/mol)	f_{PEG}[a] (wt %)	F_{PEG}[b] (wt %)	M_n[c] (10^4 g/mol)	PDI[c]	L_{PBS}
PBSEG$_{1K\text{-}36}$	1	30	36	8.70	2.83	10
PBSEG$_{1K\text{-}41}$	1	35	41	10.62	2.71	8
PBSEG$_{1K\text{-}45}$	1	40	45	8.47	2.82	7
PBSEG$_{1K\text{-}50}$	1	45	50	7.57	2.95	5
PBSEG$_{1K\text{-}57}$	1	50	57	9.11	3.14	4
PBSEG$_{2K\text{-}26}$	2	20	26	8.95	2.45	33
PBSEG$_{2K\text{-}29}$	2	25	29	12.31	2.64	28
PBSEG$_{2K\text{-}34}$	2	30	34	9.31	2.92	22
PBSEG$_{2K\text{-}39}$	2	35	39	10.61	2.70	18
PBSEG$_{2K\text{-}46}$	2	40	46	8.11	2.47	13
PBSEG$_{6K\text{-}19}$	6	15	19	8.50	2.86	148
PBSEG$_{6K\text{-}26}$	6	20	26	9.63	2.83	99
PBSEG$_{6K\text{-}29}$	6	25	29	8.83	2.52	85
PBSEG$_{6K\text{-}35}$	6	30	35	8.11	2.47	64
PBSEG$_{10K\text{-}12}$	10	10	12	9.39	2.40	426
PBSEG$_{10K\text{-}18}$	10	15	18	9.40	2.96	264
PBSEG$_{10K\text{-}24}$	10	20	24	8.91	2.78	184
PBSEG$_{10K\text{-}32}$	10	25	32	7.53	2.75	123

[a] f_{PEG} presents feed ratio of PEG diol. [b] The weight fraction of PEG segment within PBSEGs which was calculated by ^{1}H NMR spectra. [c] $M_{n,PBSEG}$ and PDI were determined by GPC with PS standards in chloroform.

Differential Scanning Calorimetry. A TA DSC-Q200 differential scanning calorimeter was employed. Samples of ~5 mg in weight were encapsulated in aluminum pans. Standard DSC heating and cooling scans were performed at 10 °C/min. Samples were first heated to 130 °C and kept at that temperature for 3 min in order to erase thermal history, then a cooling run at 10 °C/min was recorded down to −70 °C, followed by a subsequent heating run performed at the same rate.

Isothermal crystallization experiments of PEG segment within PBSEG were studied, and the detailed procedure is similar with our previous work.[46] The sample was annealed at 130 °C and equilibrated at a specified temperature. When the PBS crystallized saturation, it was quickly cooled to the chosen PEG segment crystallization temperature, and the crystallization process was recorded.

Self-nucleation experiments of PEG segment were performed. A typical procedure was as follows:[23,47−56] (i) A sample was heated to 70 °C to melt completely to erase thermal history. (ii) It was cooled at 10 °C/min to −65 °C to provide it with a standard thermal history. (iii) The sample was heated to a self-nucleation temperature around the melting temperature (T_m), denoted T_s, and isothermally kept for 3 min. (iv) After treatment at T_s, it was cooled to −65 °C at 10 °C/min, and (v) subsequently heated at the same rate until completely melting of the sample.

Atomic Force Microscope. Surface morphology of PBSEG$_{10K\text{-}32}$, PBSEG$_{10K\text{-}24}$, and PBSEG$_{10K\text{-}18}$ was studied by

dx.doi.org/10.1021/jp4059966 | J. Phys. Chem. B 2013, 117, 10665−10676

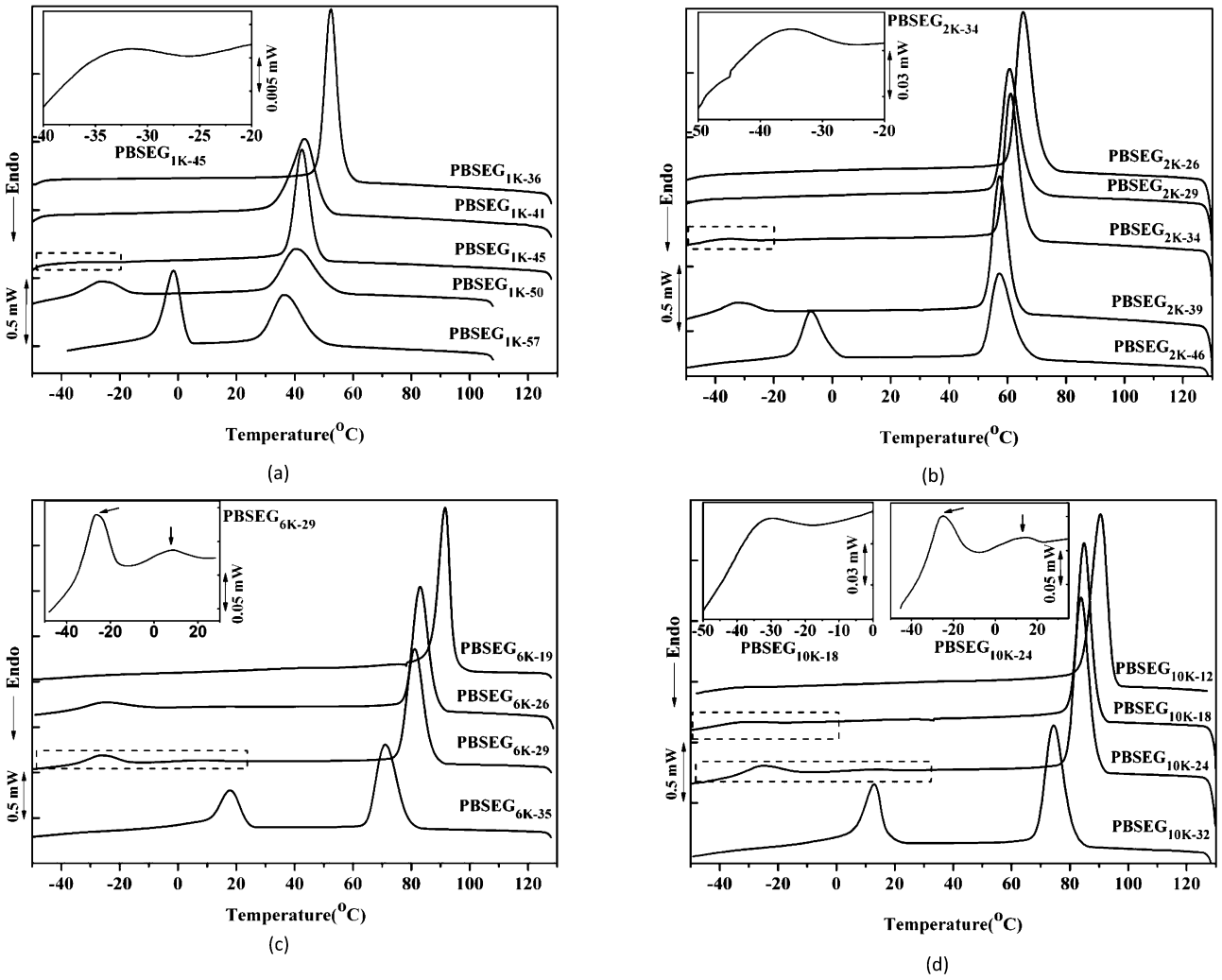

Figure 1. DSC cooling scans at 10 °C/min of (a) $PBSEG_{1K}$, (b) $PBSEG_{2K}$, (c) $PBSEG_{6K}$, and (d) $PBSEG_{10K}$ multiblock copolymers.

using Agilent Technologies 5500 atomic force microscope (Agilent Technologies Co. Ltd., USA). A definite weight of a sample was dissolved in chloroform and was spin coated on a mica sheet. Height and amplitude images of the thin layer film were obtained with a tapping mode.

RESULTS AND DISCUSSION

Standard DSC Results. Figure 1 displays the DSC cooling scans and Figure 2 displays subsequent heating scans performed at 10 °C/min for the multiblock copolymers (a), (b), (c), and (d) corresponding to PBSEG with PEG molecular weight of 1K, 2K, 6K, and 10K, respectively. The crystallization temperatures (T_c) of PEG segment within PBSEG, including cold crystallization (T_{cc}), are summarized in Table 2. For the series of $PBSEG_{1K}$ with the lowest PEG molecular weight (Figures 1a and 2a), the T_c of PEG segment varied distinctly with its content. It was found at −1.71 °C for $PBSEG_{1K\text{-}57}$, and shifted to lower temperature (−26.28 °C and −31.63 °C for $PBSEG_{1K\text{-}50}$ and $PBSEG_{1K\text{-}45}$, respectively) when the content of PEG segment decreased. Meanwhile, cold crystallizations were also observed in these two samples with T_{cc} at −29.43 °C and −25.07 °C, respectively. Additionally, we can see that crystallization enthalpy also decreased with the decrease of F_{PEG}. As for PEG segment within $PBSEG_{1K\text{-}50}$ and $PBSEG_{1K\text{-}45}$, such a large supercooling temperature needed to crystallize and occurrence of cold crystallization can be attributed to the homogeneous nucleation crystallization mechanism. The crystallization of PEG segment with high weight fraction (≥57 wt %) was nucleated by previously crystallized PBS segment spherulites, i.e., the heterogeneous nucleation mechanism, depicted in Scheme 1A. However, when the PEG segment content decreased to a certain value, PEG segments were confined in microdomains of interlamellar regions formed by previously crystallized PBS segment spherulites (Scheme 1A). In other words, PEG segments were isolated by PBS crystals and less active heterogeneities could be available for PEG crystallization. When the number of microdomains was higher than that of the heterogeneities, fractionated crystallization or homogeneous nucleation crystallization would take place. For $PBSEG_{1K}$ system, the homogeneous nucleation crystallization of PEG segment appeared when PEG content was ≤50 wt %. Detailed evidence of the nucleation mechanism are given in following sections. In addition, there was no exothermal peak when F_{PEG} reduces to 41 wt % or even lower.

When the PEG segment chain length increased to 2000 g/mol, the transition point from heterogeneous to homogeneous nucleation crystallization of PEG segment appeared at 39 wt % (illustrated in Figures 1b and 2b, and Table 2), lower than the transition point at 50% of $PBSEG_{1K}$. Unlike di- or triblock copolymers, the microstructure and confinement of PEG

dx.doi.org/10.1021/jp4059966 | J. Phys. Chem. B 2013, 117, 10665−10676

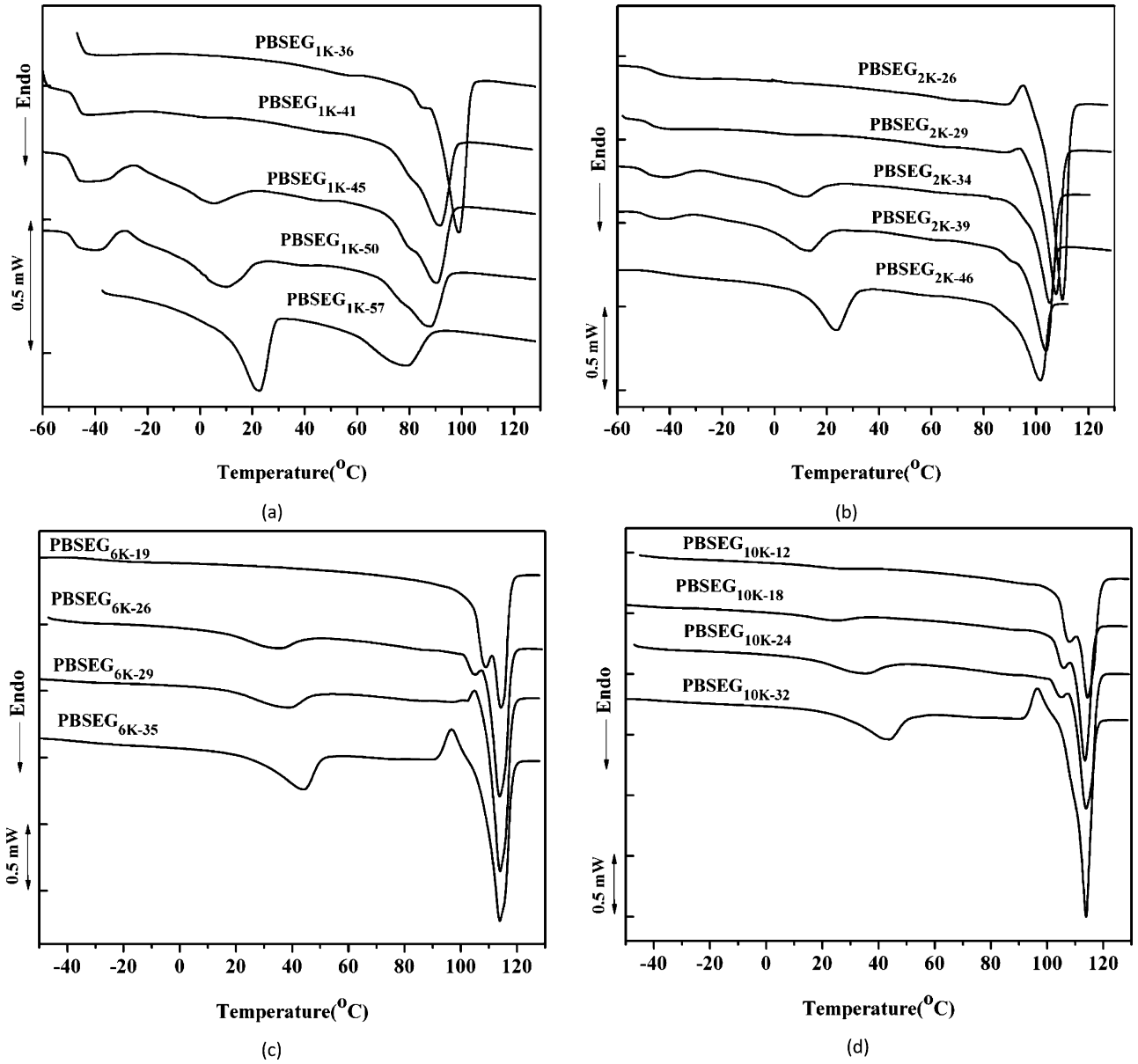

Figure 2. Subsequent heating scans after cooling runs at 10 °C/min of (a) $PBSEG_{1K}$, (b) $PBSEG_{2K}$, (c) $PBSEG_{6K}$, and (d) $PBSEG_{10K}$ multiblock copolymers.

dispersed phase in PBS matrix phase highly depends on the chain sequence as well as the segment content. From our previous work,[45] increase of PEG segment chain length while F_{PEG} was kept the same would lead to the increase of the average length of PBS segment (L_{PBS}, the values are listed in Table 1). On the one hand, the crystallizability of the PEG segment improves with increase of PEG segment chain length. On the other hand, increase of PBS chain length results in thicker PBS crystal lamella and larger spherulites.[46] Therefore, the confined degree of PEG segment between PBS crystal lamellaes reduced. As a consequence, homogeneous nucleation phenomenon took place at a lower F_{PEG} value when the PEG segment chain length increased.

Now, it is expectable that homogeneous nucleation phenomenon occurred at more lower content with further increase of PEG segment to 6000 and 10 000 g/mol. In addition, fractional crystallization took place. From Figure 1c, T_c of PEG segment within $PBSEG_{6K-35}$ was 17.75 °C, very close to that of $PBSEG_{6K-48}$ (17.88 °C) and $PBSEG_{6K-61}$ (19.16 °C) (reported in our previous work[45]), indicating that there was little change (decrease) of T_c when F_{PEG} was relative high. However, two crystallization peaks of PEG segment were detected when F_{PEG} decreased to 29 wt %, illustrated by the magnified inset in Figure 1c, suggesting the occurrence of fractional crystallization. Furthermore, only one crystallization peak at larger supercooling was observed when F_{PEG} equalled 26 wt %. With F_{PEG} further reducing to 19 wt %, PEG segment was completely free from crystallization at 10 °C/min cooling scan. The crystallization of the PEG segment within $PBSEG_{10K}$ showed similar feature with $PBSEG_{6K}$, except that the fractional crystallization phenomenon occurred at a lower content (24 wt %). In addition, there is no cold crystallization for PEG segment within $PBSEG_{6K}$ and $PBSEG_{10K}$ in the heating scans, illustrated in Figure 2c,d.

Obviously different from the direct transition of $PBSEG_{1K}$ and $PBSEG_{2K}$ from a small supercooling to a large supercooling

dx.doi.org/10.1021/jp4059966 | J. Phys. Chem. B 2013, 117, 10665−10676

Table 2. Crystallization Temperatures of PEG Segment within PBSEG Obtained from DSC Scans

sample	T_{c1}[a] (°C)	T_{c2}[a] (°C)	T_{cc}[a] (°C)	ΔH_{c1} (J/g)	ΔH_{c2} (J/g)	ΔH_{cc} (J/g)
$PBSEG_{1K-36}$	–[b]	–	–	–	–	–
$PBSEG_{1K-41}$	–	–	–	–	–	–
$PBSEG_{1K-45}$	–	−31.63	−25.07	–	0.13	4.58
$PBSEG_{1K-50}$	–	−26.28	−29.43	–	6.56	1.15
$PBSEG_{1K-57}$	−1.71	–	–	23.57	–	–
$PBSEG_{2K-26}$	–	–	–	–	–	–
$PBSEG_{2K-29}$	–	–	–	–	–	–
$PBSEG_{2K-34}$	–	−34.70	−28.56	–	0.94	3.41
$PBSEG_{2K-39}$	–	−32.09	−30.92	–	4.52	1.67
$PBSEG_{2K-46}$	−7.25	–	–	19.15	–	–
$PBSEG_{6K-19}$	–	–	–	–	–	–
$PBSEG_{6K-26}$	–	−26.37	–	–	3.64	–
$PBSEG_{6K-29}$	9.63	−26.19	–	1.79	4.57	–
$PBSEG_{6K-35}$	17.92	–	–	21.73	–	–
$PBSEG_{10K-12}$	–	–	–	–	–	–
$PBSEG_{10K-18}$	–	−30.51	–	–	1.42	–
$PBSEG_{10K-24}$	11.45	−26.05	–	0.84	3.98	–
$PBSEG_{10K-32}$	13.32	–	–	26.34	–	–

[a] T_{c1}, T_{c2}, and T_{cc} refer to the higher, lower, and cold crystallization temperatures, respectively. [b] "—" = not detected.

Scheme 1. PEG Segment Crystallization Scheme after the PBS Segment Crystallization: (A) Heterogeneous Nucleated Crystallization of PEG; (B) Fractional Crystallization of PEG; and (C) Homogeneous Nucleated Crystallization of PEG

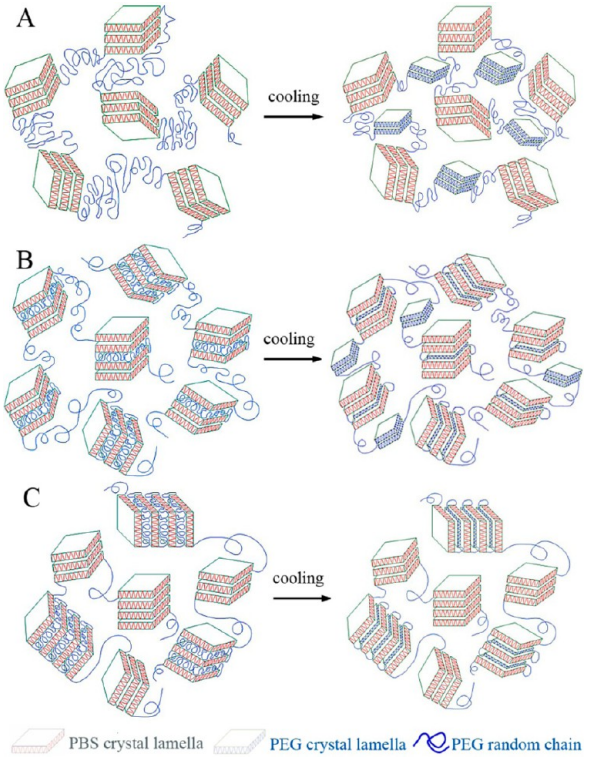

crystallization, two crystallization peaks of PEG crystallization within $PBSEG_{6K-29}$ and $PBSEG_{10K-24}$, which include both heterogeneous and homogeneous nucleation mechanism, simultaneously appear. Compared with $PBSEG_{1K}$ and $PBSEG_{2K}$, $PBSEG_{6K}$ and $PBSEG_{10K}$ possessed much longer segment chain lengths. The confined degree of PEG segment by PBS crystal lamellae reduced, which led to larger sized microdomains and fewer number of microdomains formed by the PEG segment. Thus, for the relative slight confined PEG segment, it might encounter different nanoenvironments, where some segments could be nucleated by PBS crystals and others might be free of heterogeneities, as illustrated in Scheme 1B. Consequently, we could observe the two crystallization peaks in cooling scan.

It is worth noting that fractional crystallization and homogeneous nucleation crystallzation phenomenon took place at different content values of PEG within PBSEG with different chain segment lengths. They appeared at lower content for PBSEG with longer PEG segment chain length. The transition from heterogeneous to homogeneous nucleation crystallization of the PEG segment displayed quite differently with the PEG segment chain length alternated. For the seriously confined PEG segment, the transition was direct, while fractional crystallization, which contains both heterogeneous and homogeneous nucleation phenomena, occurred for the slightly confined PEG segment. As far as the authors are aware, this is the first report that the fractional crystallization and homogeneous nucleation phenomena took place at different segment weight fraction for a crystallizable component within a miscible multiblock copolymer.

Isothermal Crystallization of PEG Segment within PBSEG. In order to further understand the nucleation mechanism and the crystallization kinetics of the PEG segment within PBSEG, the isothermal crystallization kinetics were studied and the Avrami equation was used to fit it. Details of this method are accorded in ref 46. Avrami parameters obtained are summarized in Table 3.

Table 3. Avrami Parameters of PEG Segment within PBSEG Obtained by Isothermal Crystallization at Different Temperatures

sample	T_c (°C)	n	k (min^{-n})	$t_{1/2}$ (min)	R^2
$PBSEG_{1K-36}$	−39	1.26	0.02	16.02	0.9988
$PBSEG_{1K-41}$	−30	1.61	0.05	4.90	0.9990
$PBSEG_{1K-45}$	−30	1.65	0.15	2.49	0.9970
$PBSEG_{1K-50}$	−18	1.78	0.89	0.87	0.9987
$PBSEG_{1K-57}$	−2	2.12	1.19	0.78	0.9987
$PBSEG_{2K-26}$	−35	1.10	0.03	19.78	0.9890
$PBSEG_{2K-29}$	−25	1.50	0.10	3.62	0.9995
$PBSEG_{2K-34}$	−20	1.48	0.17	2.54	0.9992
$PBSEG_{2K-39}$	−13	1.74	0.22	1.95	0.9989
$PBSEG_{2K-46}$	20	2.31	0.73	0.98	0.9996
$PBSEG_{6K-19}$	−20	1.42	0.08	4.53	0.9998
$PBSEG_{6K-26}$	−18	1.72	0.28	1.68	0.9761
$PBSEG_{6K-29}$	−10	1.67	3.20	0.37	0.9989
$PBSEG_{6K-35}$	30	1.99	0.12	2.41	0.9974
$PBSEG_{10K-12}$	−38	1.26	0.04	10.31	0.9968
$PBSEG_{10K-18}$	−20	1.42	0.09	4.17	0.9916
$PBSEG_{10K-24}$	−19	1.77	0.12	2.72	0.9962
$PBSEG_{10K-32}$	25	2.13	2.38	0.56	0.9996

From Table 3, Avrami exponents (n) of $PBSEG_{1K-57}$, $PBSEG_{2K-46}$, $PBSEG_{6K-35}$, and $PBSEG_{10K-32}$ are 2.12, 2.30, 1.99, and 2.13, respectively. According to previous study,[46] the crystallization of the PEG segment was attributed to 2D lamellar aggregates and heterogeneous nucleation within the preformed PBS spherulites. With F_{PEG} decreasing, fractional

dx.doi.org/10.1021/jp4059966 | J. Phys. Chem. B 2013, 117, 10665−10676

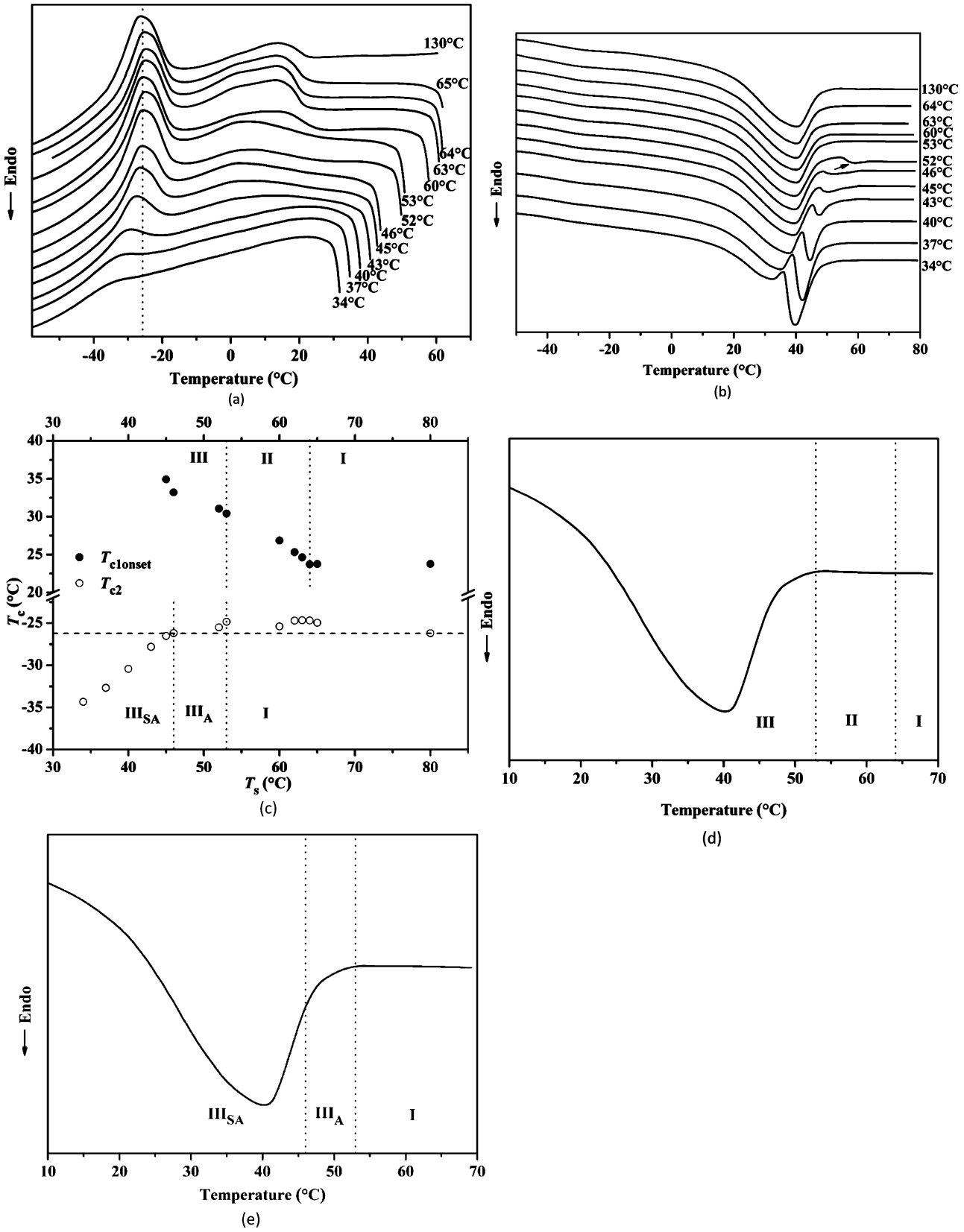

Figure 3. (a) DSC cooling scans at 10 °C/min from T_s for self-nucleation of the PEG segment within $PBSEG_{6K-29}$. (b) Subsequent heating scans at 10 °C/min. (c) T_c (including $T_{c1onset}$ and T_{c2}, see text) vs T_s of PEG segments within $PBSEG_{6K-29}$ (the dotted lines indicate changes in self-nucleation domains, and dashed lines are present to account for the variation of T_c relative to T_c of domain I). Self-nucleation domains for self-nucleation of PEG segment within $PBSEG_{6K-29}$ that crystallizes in (d) T_{c1} and (e) T_{c2} (the dotted lines indicate changes in self-nucleation domains).

dx.doi.org/10.1021/jp4059966 | J. Phys. Chem. B 2013, 117, 10665−10676

crystallization or homogeneous nucleation phenomenon of PEG segments in $PBSEG_{1K\text{-}50}$, $PBSEG_{2K\text{-}39}$, $PBSEG_{6K\text{-}29}$, and $PBSEG_{10K\text{-}24}$ occurred. Due to fractional crystallization or homogeneous nucleation phenomenon, the values of n reduced to 1.78, 1.74, 1.67, and 1.77, respectively. When F_{PEG} further decreased, the Avrami exponents of the PEG segment within $PBSEG_{1K\text{-}36}$, $PBSEG_{2K\text{-}26}$, $PBSEG_{6K\text{-}19}$, and $PBSEG_{10K\text{-}12}$ obtained were 1.26, 1.10, 1.42, and 1.26, respectively. This decrease of n can be reckoned as the dimensional reduction of the PEG segment's growth due to more PBS crystals being previously formed. Avrami exponents of $PBSEG_{1K\text{-}36}$, $PBSEG_{2K\text{-}26}$, $PBSEG_{6K\text{-}19}$, and $PBSEG_{10K\text{-}12}$ were approximated to 1, called a first-order overall crystallization kinetics. That was strong evidence for homogeneous nucleation crystallization,[19,22,44,57,58] which means the crystal growth from the nucleus to the interphase can be regarded as instantaneous,[46] or the kinetics is entirely controlled by the nucleation process for the PEG crystallization in $PBSEG_{1K\text{-}36}$, $PBSEG_{2K\text{-}26}$, $PBSEG_{6K\text{-}19}$, and $PBSEG_{10K\text{-}12}$. The PEG segments with homogeneous nucleation crystallized in PEG microdomains, isolated by previous PBS crystals without heterogeneities. It is worth noting that the crystallization of PEG segments occurred at a very large supercooling, a few degrees above the glass transition temperature (T_g) of $PBSEG_{1K\text{-}36}$, $PBSEG_{2K\text{-}26}$, and $PBSEG_{10K\text{-}12}$ (the value of T_g ranges from 42 to 49 °C for all samples). Thus, we are convinced that the crystallization mechanism of the PEG segments within $PBSEG_{1K\text{-}36}$, $PBSEG_{2K\text{-}26}$, $PBSEG_{6K\text{-}19}$, and $PBSEG_{10K\text{-}12}$ was indeed homogeneous nucleation.

An interesting phenomenon observed in Table 3 is that the values of crystallization half-time ($t_{1/2}$) were rather high at large supercoolings for $PBSEG_{1K\text{-}36}$ (16.02 min, at −39 °C), $PBSEG_{2K\text{-}26}$ (19.78 min, at −35 °C), $PBSEG_{6K\text{-}19}$ (4.53 min, at −20 °C), and $PBSEG_{10K\text{-}12}$ (10.31 min, at −38 °C). This meant a very slow overall crystallization rate for the PEG crystallization of these four samples. From the above discussions, we know that the kinetics is dominated by nucleation when the Avrami exponent is generally close to 1. We could use the Turnbull and Fisher equation[59] to analyze the nucleation process. The equation is written as follows

$$I^* = (NkT/h)\exp[-(\Delta G^* + \Delta G_\eta)/kT] \quad (1)$$

where I^* is nucleation rate, N refers to the number of noncrystallization chains that can join in a single nucleation step, ΔG^* is the free energy for the formation of a critical size nucleus, and ΔG_η is the free energy of crystallizable chains through the interphase for a short-range diffusion. The nucleation process is determined by two factors: the first one is ΔG^* that decreases with the supercooling, and the second one is ΔG_η, a constant parameter at high temperatures, while it increases significantly as temperature approaches T_g. As the isothermal crystallization temperature of PEG segments approached T_g, the slow overall crystallization rate could be interpreted as a very slow nucleation rate due to the significant increase in ΔG_η.

Self-Nucleation of PEG Segment within PBSEG. The self-nucleation experiment was employed to study the effect of self-nuclei on the crystallization behavior of PEG segments. In general, depending on the values of T_s, the temperature range is divided into three domains. When T_s is high enough to melt molecular chain completely, where the nucleation density is constant, the sample is in domain I, or called "complete-melting domain". When T_s is high enough to melt almost all crystals while low enough to produce self-seeds, nucleation density can be extremely increased, and the sample is located in domain II or "self-nucleation domain". When T_s is low to partially melt the sample and to induce annealing peak of unmelted crystals, then the sample is in domain III or "self-nucleation and annealing domain (III_{SA})".

Due to the two crystallization temperatures of the PEG segment containing both heterogeneous and homogeneous nucleation crystallization mechanisms, we first investigated the interesting samples $PBSEG_{6K\text{-}29}$ and $PBSEG_{10K\text{-}24}$, which could reveal the different self-nucleation behaviors between heterogeneous and homogeneous nucleation mechanisms in different nanoenvironments. Figure 3a shows DSC cooling scans after different T_s isothermal treatments of $PBSEG_{6K\text{-}29}$. The two crystallization temperatures in standard cooling scan were noted as T_{c1} (9.63 °C) and T_{c2} (−26.19 °C), respectively (Table 2). Figure 3a,b displays the cooling scans after self-nucleation and subsequent heating scans of PEG segment within $PBSEG_{6K\text{-}29}$. Since T_{c1} shows irregular shape, the peak positions cannot be accurately located, and thus we use the onset of the crystallization temperature (noted by $T_{c1onset}$) to represent the level of crystallization temperature. From Figure 3a, $T_{c1onset}$ of the PEG segment during cooling did not change when T_s was equal to or higher than 64 °C. That meant that the nucleation density kept at a constant, and no new nuclei were generated after 3 min at such temperatures due to the complete melting of the segment. Therefore, the PEG segment was considered to be under domain I when $T_s \geq 64$ °C. When T_s was lowered to 63 °C, a small increase of $T_{c1onset}$ could be observed, indicating the PEG segment was self-nucleated and PEG nucleation density increased. This change can be illustrated more clearly in the curve of T_c versus T_s (upper part of Figure 3c). Thus, domain II starts at T_s = 63 °C. When T_s = 52 °C, a small high-temperature melting peak appeared in the heating scan (annealing peak, indicated with an arrow in Figure 3b), which was a typical feature of domain III. The appearance of annealing phenomenon after self-nucleation was attributed to the incomplete melting of PEG crystals. With further decrease of T_s, $T_{c1onset}$ continued to increase until $T_{c1onset}$ could not be clearly marked since crystallization occurred immediately upon cooling. The remaining molten fraction of PEG was completely self-nucleated by annealed crystals when T_s was lower than 40 °C, where crystallization took place immediately upon cooling. Besides, more amount of unmelted fraction at T_s remained with decrease of T_s, as indicated by enthalpy increase of the higher melting temperature endotherm (see curves in Figure 3b). At the same time, the higher melting temperature also moved to lower values. A schematic illustration of the location of the three domains is given in Figure 3d. Classical self-nucleation domains proved T_{c1} of the PEG segment within $PBSEG_{6K\text{-}29}$ as the heterogeneous nucleation mechanism once again.

T_{c2} of the PEG segment within $PBSEG_{6K\text{-}29}$ did not show classical self-nucleation behavior. The plots of T_{c2} versus T_s of PEG segment within $PBSEG_{6K\text{-}29}$ are schemed in Figure 3c (the lower part). Small fluctuations of T_{c2} were observed when T_s was above 46 °C, which might be some uncertainties in data evaluation due to very small heat of crystallization.[51] Slight increase of T_{c2} was observed even when T_s decreased to annealing domain of T_{c1} (52 °C). That meant the high concentration of self-seeds for T_{c1} was not able to self-nucleate T_{c2} of PEG segment. These results suggested that domain II of T_{c2} disappeared. When the nucleation mechanism of the PEG

dx.doi.org/10.1021/jp4059966 | J. Phys. Chem. B 2013, 117, 10665−10676

segment is homogeneous nucleation, the annealing domain was called domain III_a in the literature.[51,60,61] In other words, the sample gets directly across from domain I to domain III_A without going through domain II. When T_s decreased to 45 °C, the crystallization temperature at T_{c2} started to decrease compared with standard cooling, indicating domain III_{SA} was reached (Figure 3e). T_{c2} shifted to much lower temperature and its enthalpy reduced progressively with decrease of T_s. When T_s decreased to a certain degree that only thin crystals (the crystallization occurred at T_{c2}) could be molten at T_s, these melted chains would crystallize at much lower temperatures under subsequent cooling. With further decrease of T_s, thinner and thinner crystals remained and the exotherm peak (including the cold crystallization) almost disappeared when T_s = 34 °C. This feature was contradictory to the sharp increase of nucleation density induced by self-nuclei, indicating that it is homogeneous nucleation mechanism for the PEG segment crystallizing at T_{c2}. Self-nucleation behavior of PEG segment within $PBSEG_{10K-24}$ shows the same feature with $PBSEG_{6K-29}$, and the results are shown here for brevity.

Compared with $PBSEG_{6K-29}$ and $PBSEG_{10K-24}$, T_c of the PEG segment within $PBSEG_{6K-35}$ was at high temperature (17.75 °C) due to higher PEG fractions, attributed to heterogeneous nucleation crystallization. As a control, self-nucleation of PEG segment within $PBSEG_{6K-35}$ was studied. For brevity, the DSC cooling and subsequent heating scans are not shown here, and the results of self-nucleation domains are displayed in Figure 4a. It shows the characteristic three domains.

Due to direct transition from heterogeneous to homogeneous nucleation mechanism of the PEG segment, self-nucleation study of the $PBSEG_{2K}$ and $PBSEG_{1K}$ systems is necessary. Self-nucleation behavior of PEG segment within $PBSEG_{2K-46}$, $PBSEG_{2K-39}$ and $PBSEG_{1K-57}$, $PBSEG_{1K-50}$ was studied. Investigation of the results of $PBSEG_{2K-46}$ showed three classical domains with domain II at 42 °C and domain III at 30 °C, respectively, depicted in Figure 4b. Heterogeneous nucleation mechanism of PEG segment within $PBSEG_{2K-46}$ can be convinced. In addition, the self-nucleation behavior study of PEG segment within $PBSEG_{2K-39}$ is displayed in Figure 5. When T_s decreased to 21 °C, T_c began to decrease and the annealing peak in the heating scan occurred simultaneously. Only the thinner crystals melted when T_s decreased, and thus T_c and the value of enthalpy (or relative area) became lower and lower (Figure 5, a, b, and d). Furthermore, the crystallization peak and cold crystallization peak almost disappeared when T_s = 12 °C. Self-nucleation domains of PEG segment within $PBSEG_{2K-39}$ are depicted in Figure 5c. The absence of domain II was attributed to the homogeneous nucleation mechanism of the PEG segment. For the $PBSEG_{1K}$ series, classical three domains were clearly present in $PBSEG_{1K-57}$, and the absence of domain II in $PBSEG_{1K-50}$ claimed the homogeneous nucleation mechanisms of the PEG segment (the results are not shown here). Due to $PBSEG_{2K-34}$ and $PBSEG_{1K-45}$ having similar features as $PBSEG_{2K-39}$ and $PBSEG_{1K-50}$, respectively, their self-nucleation behavior was not investigated. It is worth noting that the self-nucleation behavior of the PEG segment at large supercooling (T_{c2}) within $PBSEG_{2K-39}$ displays differently from that of $PBSEG_{6K-29}$, and the absence of III_A $PBSEG_{2K-39}$ may be caused by the complex of multiblock copolymers.

Atomic Force Microscope. In order to further investigate the influence of PBS crystals on crystallization and melting of the PEG segment, the surface morphology of $PBSEG_{10K}$ before

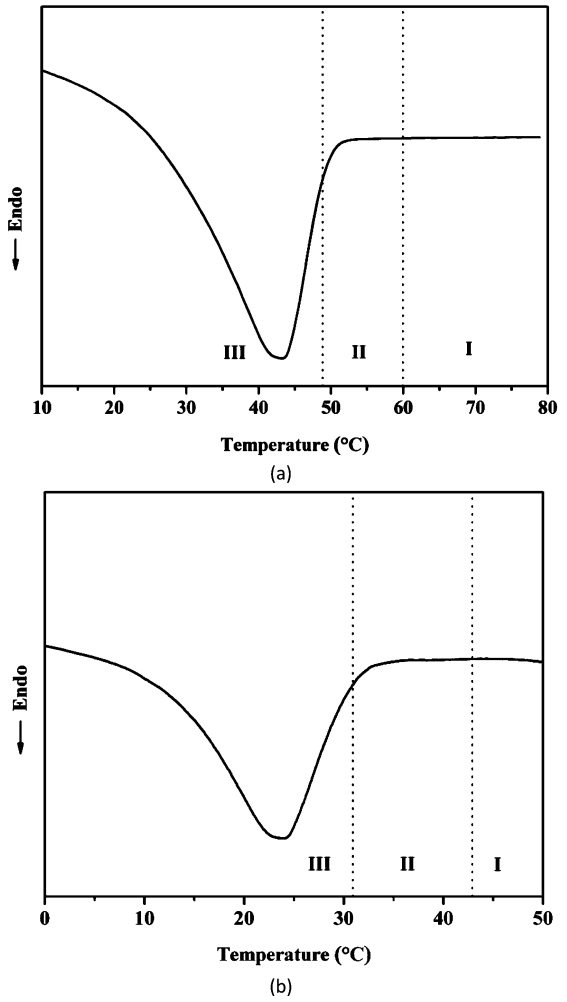

Figure 4. (a) Self-nucleation domains for self-nucleation of PEG segment within $PBSEG_{6K-35}$. (b) Self-nucleation domains for self-nucleation of PEG segment within $PBSEG_{2K-46}$.

and after melting of PEG segment was observed by AFM as an example (Figures 6, 7, and 8). Figure 6, a and b, is the AFM amplitude images of $PBSEG_{10K-32}$ at room temperature and 70 °C, respectively. It can be seen clearly that the morphology changed evidently after melting of the PEG segment. The height images, illustrated in Figure 6a′,b′, still witnessed remarkable changes with melting of the PEG segment. The flat-on lamellar crystals around the boundary of two spherulites, circled in Figure 6a,b, obviously disappeared. We could find little morphology trace about the preheating situation. This was because the PEG segment with high segment content was nucleated by previous PBS crystals. With F_{PEG} decreasing to 24 wt %, i.e., $PBSEG_{10k-24}$, though there were some changes of surface morphology with melting of the PEG segment, the main structure of morphology almost kept unchanged (Figure 7a,b), and those changes could be seen more clearly in the magnified images in Figure 7a′,b′. With the heating process to 65 °C, almost only edge-on lamellae were left and the much smaller flat-on lamellae between the edge-on lamellae missed with the rise of temperature. Thus, we could infer that some of the PEG segment within $PBSEG_{10k-24}$ was confined in the interlamellar regions of previously crystallized PBS segment spherulites. When F_{PEG} was further lowered to 18 wt %, we could observe that the macromorphology underwent an imperceptible change

dx.doi.org/10.1021/jp4059966 | J. Phys. Chem. B 2013, 117, 10665−10676

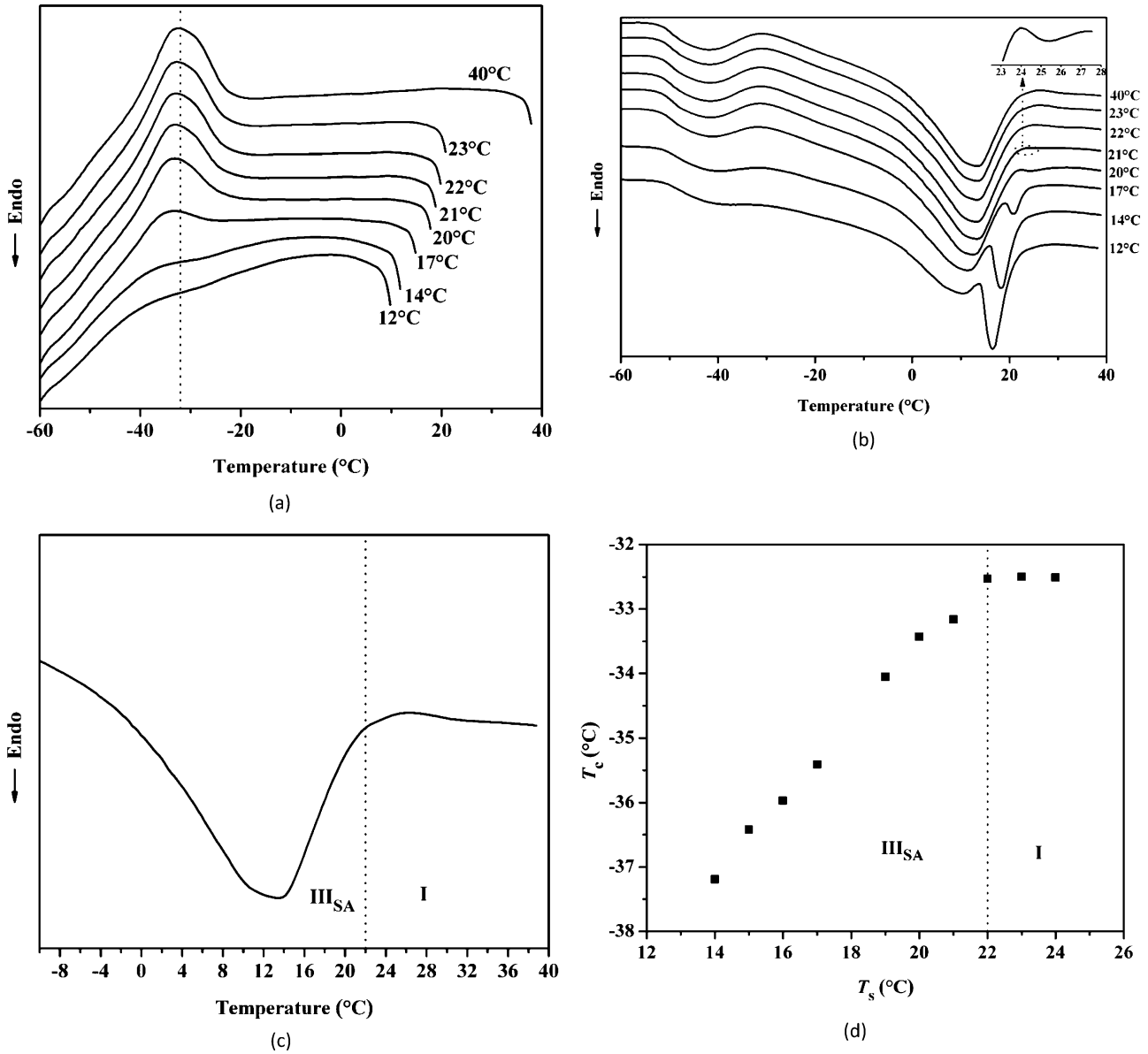

Figure 5. (a) DSC cooling scans at 10 °C/min from T_s for self-nucleation of the PEG segment within $PBSEG_{2K\text{-}39}$. (b) Subsequent heating scans at 10 °C/min. (c) Self-nucleation domains for self-nucleation of PEG segment within $PBSEG_{2K\text{-}39}$. (d) Crystallization temperatures of the PEG segment within $PBSEG_{2K\text{-}39}$ vs T_s. The dotted lines indicate changes in self-nucleation domains.

(Figure 8a,b). In order to understand the micromorphology, magnified images are shown in Figure 8a′,b′. Some edge-on lamellae could be seen more clearly after the temperature rose to 45 °C. The PEG segments were completely confined in edge-on lamellae of PBS, proving the fact that T_c of the PEG segment within $PBSEG_{10K\text{-}18}$ occurred at large supercooling. Morphology of $PBSEG_{10K\text{-}12}$ did not change with temperature rising to 55 °C since the PEG segment did not crystallize, and the results are not shown here for brevity. Additionally, there was gradual decrease of the spherulite size with decrease of the PEG content, which accorded with our previous work.

CONCLUSIONS

In summary, we have investigated the fractional crystallization, homogeneous nucleation of the PEG segment, and self-nucleation behavior of the PEG segment within miscible double crystalline PBSEG multiblock copolymers. The crystallization behaviors of PBSEG highly depended on chain segment length and chain sequence distribution as well as composition of the copolymers. In detail, $PBSEG_{6K\text{-}29}$ and $PBSEG_{10K\text{-}24}$ exhibited a marked fractional crystallization phenomenon, as indicated by the double crystallization exotherm of the PEG segment at T_{c1} and T_{c2}, respectively. T_{c1} was attributed to the crystallization after heterogeneous nucleation by previous PBS crystals or other heterogeneities, since it appeared at relative low supercooling. T_{c2}, at a large supercooling temperature, was homogeneous nucleation crystallization. Only the low crystallization temperature and cold crystallization temperature of PEG segment occurred in $PBSEG_{2k\text{-}39}$ and $PBSEG_{1K\text{-}50}$, which transferred directly from heterogeneous to homogeneous nucleation mechanism caused by more seriously confined of PEG segment within the PBS crystals. Nucleation mechanism was further proved by isothermal crystallization and self-nucleation investigation. For the PEG segment within $PBSEG_{1K\text{-}36}$, $PBSEG_{2K\text{-}26}$, $PBSEG_{6K\text{-}19}$, and $PBSEG_{10K\text{-}12}$, the results that Avrami exponent was close to

dx.doi.org/10.1021/jp4059966 | J. Phys. Chem. B 2013, 117, 10665−10676

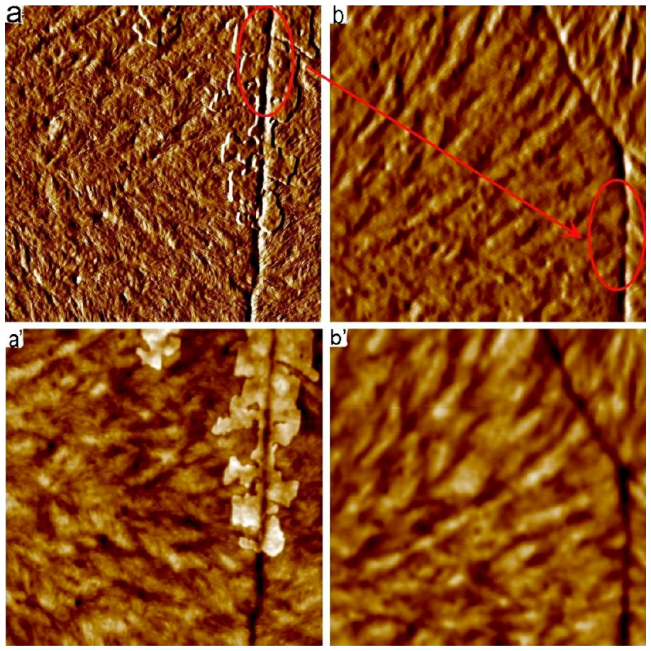

Figure 6. AFM amplitude images of $PBSEG_{10K\text{-}32}$ (a) at room temperature and (b) at 70 °C; AFM height images of the same sample (a′) at room temperature and (b′) at 70 °C. The scanning scope is 5 μm.

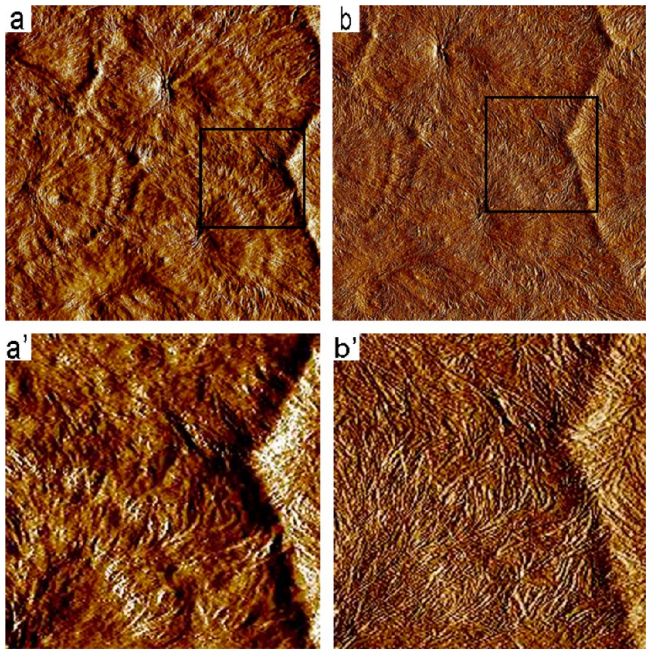

Figure 7. AFM amplitude images of $PBSEG_{10K\text{-}24}$ (a) at room temperature and (b) at 65 °C; magnified AFM height images (a′) of square box in (a) and (b′) of square box in (b). The scanning scope is 5 μm for (a) and (b).

1 and great supercooling (near to T_g) was needed to crystallize indicated the nucleation mechanism of the PEG segment was homogeneous nucleation and the PEG segment was confined in isolated microdomains. Self-nucleation behavior of T_{c1} of the PEG segment within $PBSEG_{6K\text{-}29}$ and $PBSEG_{10K\text{-}24}$ showed typical three-domain self-nucleation behavior. However, crystals that arose from homogeneous nuclei could not be nucleated by these self-seeds in classical domain II, thus domain II of PEG

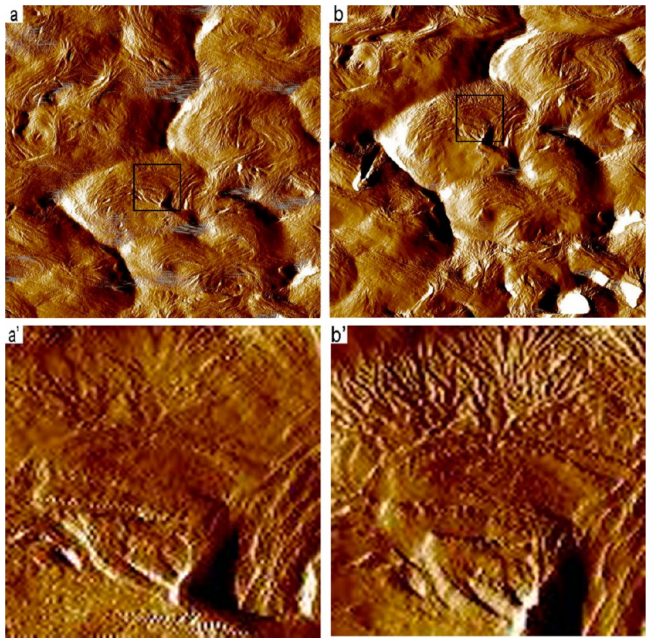

Figure 8. AFM amplitude images of $PBSEG_{10K\text{-}18}$ (a) at room temperature and (b) at 45 °C; magnified AFM height images (a′) of square box in (a) and (b′) of square box in (b). The scanning scope is 5 μm for (a) and (b).

segment crystallizing at T_{c2} disappeared. The direct transition from heterogeneous to homogeneous nucleation mechanism of PEG segment within $PBSEG_{1K}$ and $PBSEG_{2K}$ was evidenced by self-nucleation investigation. AFM morphology observation showed the confined degree of PEG segment by previous PBS crystals was profoundly influenced by segment fraction. The confinement of PEG segment by previous PBS edge-on lamellaes was observed in the sample which performs a homogeneous nucleation crystallization behavior.

AUTHOR INFORMATION

Corresponding Author

*Fax: +86-28-85410284. Tel.: +86-28-85410755. E-mail: kkyangscu@126.com.

Notes

The authors declare no competing financial interest.

ACKNOWLEDGMENTS

This work was supported financially by the National Science Foundation of China (51273120, 51121001), Program of International S & T Cooperation (2011DFA51420), and Program for Changjiang Scholars and Innovative Research Team in University of the Ministry of Education of China (IRT1026). The authors also thank the Prof. Shou-Ke Yan in Beijing University of Chemical Technology for the help with the AFM measurements.

REFERENCES

(1) Bogdanov, B.; Vidts, A.; Schacht, E.; Berghmans, H. Isothermal Crystallization of Poly(ε-caprolactone−ethylene glycol) Block Copolymers. *Macromolecules* **1999**, *32*, 726−731.

(2) Alizadeh, A.; Richardson, L.; Xu, J.; McCartney, S.; Marand, H.; Cheung, Y. W.; Chum, S. Influence of Structural and Topological Constraints on the Crystallization and Melting Behavior of Polymers. 1. Ethylene/1-Octene Copolymers. *Macromolecules* **1999**, *32*, 6221−6235.

(3) He, Y.; Zhu, B.; Kai, W.; Inoue, Y. Effects of Crystallization Condition of Poly(butylene succinate) Component on the Crystallization of Poly(ethylene oxide) Component in Their Miscible Blends. *Macromolecules* **2004**, *37*, 8050−8056.
(4) Ho, R. M.; Chiang, Y.-W.; Lin, C. C.; Huang, B. H. Crystallization and Melting Behavior of Poly(ε-caprolactone) under Physical Confinement. *Macromolecules* **2005**, *38*, 4769−4779.
(5) Rahman, N.; Kawai, T.; Matsuba, G.; Nishida, K.; Kanaya, T.; et al. Effect of Polylactide Stereocomplex on the Crystallization Behavior of Poly(l-lactic acid). *Macromolecules* **2009**, *42*, 4739−4745.
(6) Hamley, I. W.; Fairclough, J. P. A.; Bates, F. S.; Ryan, A. J. Crystallization thermodynamics and kinetics in semicrystalline diblock copolymers. *Polymer* **1998**, *39*, 1429−1437.
(7) Qiu, Z.; Ikehara, T.; Nishi, T. Poly(hydroxybutyrate)/poly(butylene succinate) blends: miscibility and nonisothermal crystallization. *Polymer* **2003**, *44*, 2503−2508.
(8) Qiu, Z.; Ikehara, T.; Nishi, T. Crystallization behaviour of biodegradable poly(ethylene succinate) from the amorphous state. *Polymer* **2003**, *44*, 5429−5437.
(9) Nojima, S.; Akutsu, Y.; Akaba, M.; Tanimoto, S. Crystallization behavior of poly([epsilon]-caprolactone) blocks starting from polyethylene lamellar morphology in poly([epsilon]-caprolactone)-block-polyethylene copolymers. *Polymer* **2005**, *46*, 4060−4067.
(10) Zhang, J.; Sato, H.; Furukawa, T.; Tsuji, H.; Noda, I.; Ozaki, Y. Crystallization Behaviors of Poly(3-hydroxybutyrate) and Poly(l-lactic acid) in Their Immiscible and Miscible Blends. *J. Phys. Chem. B* **2006**, *110*, 24463−24471.
(11) Yan, C.; Zhang, Y.; Hu, Y.; Ozaki, Y.; Shen, D.; Gan, Z.; Yan, S.; Takahashi, I. Melt Crystallization and Crystal Transition of Poly(butylene adipate) Revealed by Infrared Spectroscopy. *J. Phys. Chem. B* **2008**, *112*, 3311−3314.
(12) Zhao, K.; Deng, Y.; Chen, G. Effects of surface morphology on the biocompatibility of polyhydroxyalkanoates. *Biochem. Eng. J.* **2003**, *16*, 115−123.
(13) Han, S. I.; Kang, S. W.; Kim, B. S.; Im, S. S. A Novel Polymeric Ionomer as a Potential Biomaterial: Crystallization Behavior, Degradation, and In-Vitro Cellular Interactions. *Adv. Funct. Mater.* **2005**, *15*, 367−374.
(14) Gan, Z.; Abe, H.; Doi, Y. Crystallization, Melting, and Enzymatic Degradation of Biodegradable Poly(butylene succinate-co-14 mol ethylene succinate) Copolyester. *Biomacromolecules* **2001**, *2*, 313−321.
(15) Gan, Z.; Abe, H.; Kurokawa, H.; Doi, Y. Solid-State Microstructures, Thermal Properties, and Crystallization of Biodegradable Poly(butylene succinate) (PBS) and Its Copolyesters. *Biomacromolecules* **2001**, *2*, 605−613.
(16) Papageorgiou, G. Z.; Bikiaris, D. N. Synthesis, Cocrystallization, and Enzymatic Degradation of Novel Poly(butylene-co-propylene succinate) Copolymers. *Biomacromolecules* **2007**, *8*, 2437−2449.
(17) Yang, Y.; Qiu, Z. Crystallization kinetics and morphology of biodegradable poly(butylene succinate-co-ethylene succinate) copolyesters: effects of comonomer composition and crystallization temperature. *CrystEngComm* **2011**, *13*, 2408−2417.
(18) Hamley, I. *Crystallization in Block Copolymers Interfaces Crystallization Viscoelasticity*; Springer: Berlin, 1999.
(19) Müller, A. J.; Balsamo, V.; Arnal, M. L. Nucleation and Crystallizationin Diblock and Triblock Copolymers. *Adv. Polym. Sci.* **2005**, *190*, 1−63.
(20) Nandan, B.; Hsu, J. Y.; Chen, H. L. Crystallization behavior of crystalline-amorphous diblock copolymers consisting of a rubbery amorphous block. *Polym. Rev.* **2006**, *46*, 143−172.
(21) Müller, A.; Arnal, M.; Balsamo, V. Crystallization in Block Copolymers with More than One Crystallizable Block. In *Progress in Understanding of Polymer Crystallization*; Springer: Berlin, 2007.
(22) Castillo, R. V.; Müller, A. J. Crystallization and morphology of biodegradable or biostable single and double crystalline block copolymers. *Prog. Polym. Sci.* **2009**, *34*, 516−560.
(23) Arnal, M. L.; Matos, M. E.; Morales, R. A.; Santana, O. O.; Müuller, A. J. Evaluation of the fractionated crystallization of dispersed polyolefins in a polystyrene matrix. *Macromol. Chem. Phys.* **1998**, *199*, 2275−2288.
(24) He, Y.; Zhu, B.; Kai, W.; Inoue, Y. Nanoscale-Confined and Fractional Crystallization of Poly(ethylene oxide) in the Interlamellar Region of Poly(butylene succinate). *Macromolecules* **2004**, *37*, 3337−3345.
(25) Cormia, R. L.; Price, F. P.; Turnbull, D. Kinetics of Crystal Nucleation in Polyethylene. *J. Chem. Phys.* **1962**, *37*, 1333−1341.
(26) Frensch, H.; Jungnickel, B. J. Some novel crystallization kinetic peculiarities in finely dispersing polymer blends. *Colloid Polym. Sci.* **1989**, *267*, 16−2727.
(27) Frensch, H.; Jungnickel, B. J. Fractionated and self-seeded crystallization in incompatible polymer blends. *Plast. Rubber Compos. Process. Appl.* **1991**, *16*, 5−10.
(28) Arnal, M. L.; Müller, A. J. Fractionated crystallisation of polyethylene and ethylene/α-olefin copolymers dispersed in immiscible polystyrene matrices. *Macromol. Chem. Phys.* **1999**, *200*, 2559−2576.
(29) Tol, R. T.; Mathot, V. B. F.; Groeninckx, G. Confined crystallization phenomena in immiscible polymer blends with dispersed micro − and nanometer sized PA6 droplets, part 1: uncompatibilized PS/PA6, (PPE/PS)/PA6 and PPE/PA6 blends. *Polymer* **2005**, *46*, 369−382.
(30) Tol, R. T.; Mathot, V. B. F.; Groeninckx, G. Confined crystallization phenomena in immiscible polymer blends with dispersed micro- and nanometer sized PA6 droplets, part 2: reactively compatibilized PS/PA6 and (PPE/PS)/PA6 blends. *Polymer* **2005**, *46*, 383−396.
(31) Tol, R. T.; Mathot, V. B. F.; Groeninckx, G. Confined crystallization phenomena in immiscible polymer blends with dispersed micro- and nanometer sized PA6 droplets, part 3: crystallization kinetics and crystallinity of micro- and nanometer sized PA6 droplets crystallizing at high supercoolings. *Polymer* **2005**, *46*, 2955−2965.
(32) Tol, R. T.; Mathot, V. B. F.; Reynaers, H.; Goderis, B.; Groeninckx, G. Confined crystallization phenomena in immiscible polymer blends with dispersed micro-and nanometer sized PA6 droplets part 4: polymorphous structure and (meta)-stability of PA6 crystals formed in different temperature regions. *Polymer* **2005**, *46*, 2966−2977.
(33) Arnal, M. L.; Balsamo, V.; López-Carrasquero, F.; Contreras, J.; Carrillo, M.; Schmalz, H.; Abetz, V.; Laredo, E.; Müller, A. J. Synthesis and Characterization of Polystyrene-b-poly(ethylene oxide)-b-poly(ε-caprolactone) Block Copolymers. *Macromolecules* **2001**, *34*, 7973−7982.
(34) Albuerne, J.; Márquez, L.; Müller, A. J.; Raquez, J. M.; Degée, P.; Dubois, P.; Castelletto, V.; Hamley, I. W. Nucleation and Crystallization in Double Crystalline Poly(p-dioxanone)-b-poly(ε-caprolactone) Diblock Copolymers. *Macromolecules* **2003**, *36*, 1633−1644.
(35) Weimann, P. A.; Hajduk, D. A.; Chu, C.; Chaffin, K. A.; Brodil, J. C.; Bates, F. S. Crystallization of tethered polyethylene in confined geometries. *J. Polym. Sci., Part B: Polym. Phys.* **1999**, *37*, 2053−2068.
(36) Loo, Y.-L.; Register, R. A.; Ryan, A. J. Polymer Crystallization in 25-nm Spheres. *Phys. Rev. Lett.* **2000**, *84*, 4120−4123.
(37) Chen, H.-L.; Hsiao, S.-C.; Lin, T.-L.; Yamauchi, K.; Hasegawa, H.; Hashimoto, T. Microdomain-Tailored Crystallization Kinetics of Block Copolymers. *Macromolecules* **2001**, *34*, 671−674.
(38) Chen, H.-L.; Wu, J.-C.; Lin, T.-L.; Lin, J. S. Crystallization Kinetics in Microphase-Separated Poly(ethylene oxide)-block-poly(1,4-butadiene). *Macromolecules* **2001**, *34*, 6936−6944.
(39) Sun, L.; Liu, Y.; Zhu, L.; Hsiao, B. S.; Avila-Orta, C. A. Self-assembly and crystallization behavior of a double-crystalline polyethylene-block-poly(ethylene oxide) diblock copolymer. *Polymer* **2004**, *45*, 8181−8193.
(40) Zhao, L.; Kai, W.; He, Y.; Zhu, B.; Inoue, Y. Effect of aging on fractional crystallization of poly(ethylene oxide) component in poly(ethylene oxide)/poly(3-hydroxybutyrate) blends. *J. Polym. Sci., Part B: Polym. Phys.* **2005**, *43*, 2665−2676.

(41) Yang, J.; Pan, P.; Hua, L.; Zhu, B.; Dong, T.; Inoue, Y. Polymorphic Crystallization and Phase Transition of Poly(butylene adipate) in Its Miscible Crystalline/Crystalline Blend with Poly(vinylidene fluoride). *Macromolecules* **2010**, *43*, 8610−8618.
(42) Yang, J.; Pan, P.; Hua, L.; Feng, X.; Yue, J.; Ge, Y.; Inoue, Y. Effects of Crystallization Temperature of Poly(vinylidene fluoride) on Crystal Modification and Phase Transition of Poly(butylene adipate) in Their Blends: A Novel Approach for Polymorphic Control. *J. Phys. Chem. B* **2012**, *116*, 1265−1272.
(43) He, C.; Sun, J.; Ma, J.; Chen, X.; Jing, X. Composition Dependence of the Crystallization Behavior and Morphology of the Poly(ethylene oxide)-poly(ε-caprolactone) Diblock Copolymer. *Biomacromolecules* **2006**, *7*, 3482−3489.
(44) Castillo, R. V. n.; Müller, A. J.; Raquez, J. M.; Dubois, P. Crystallization Kinetics and Morphology of Biodegradable Double Crystalline PLLA-b-PCL Diblock Copolymers. *Macromolecules* **2010**, *43*, 4149−4160.
(45) Huang, C. L.; Jiao, L.; Zhang, J. J.; Zeng, J. B.; Yang, K. K.; Wang, Y. Z. Poly(butylene succinate)-poly(ethylene glycol) multiblock copolymer: Synthesis, structure, properties and shape memory performance. *Polym. Chem.* **2012**, *3*, 800−808.
(46) Huang, C. L.; Jiao, L.; Zeng, J. B.; Zhang, M.; Xiao, L. P.; Yang, K. K.; Wang, Y. Z. Crystallization behavior and morphology of double crystalline poly(butylene succinate)-poly(ethylene glycol) multiblock copolymers. *Polymer* **2012**, *53*, 3780−3790.
(47) Müller, A.; Hernández, Z.; Arnal, M.; Sánchez, J. Successive self-nucleation/annealing (SSA): A novel technique to study molecular segregation during crystallization. *Polym. Bull.* **1997**, *39*, 465−472.
(48) Balsamo, V.; Paolini, Y.; Ronca, G.; Müller, A. J. Crystallization of the polyethylene block in polystyrene-b-polyethylene-b-polycaprolactone triblock copolymers, 1. Self-nucleation behavior. *Macromol. Chem. Phys.* **2000**, *201*, 2711−2720.
(49) Müller, A. J.; Arnal, M. L.; López-Carrasquero, F. Nucleation and crystallization of PS-b-PEO-b-PCL triblock copolymers. *Macromol. Symp.* **2002**, *183*, 199−204.
(50) Schmalz, H.; Abetz, V.; Müller, A. J. Thermal and self-nucleation behavior of molecular complexes formed by p-nitrophenol and the poly(ethylene oxide) end block within an ABC triblock copolymer. *Macromol. Symp.* **2002**, *183*, 179−184.
(51) Schmalz, H.; Müller, A. J.; Abetz, V. Crystallization in ABC Triblock Copolymers with Two Different Crystalline End Blocks: Influence of Confinement on Self-Nucleation Behavior. *Macromol. Chem. Phys.* **2003**, *204*, 111−124.
(52) Müller, A. J.; Albuerne, J.; Esteves, L. M.; Marquez, L.; Raquez, J.-M.; Degée, P.; Dubois, P.; Collins, S.; Hamley, I. W. Confinement Effects on the Crystallization Kinetics and Self-Nucleation of Double Crystalline Poly(p-dioxanone)-b-poly(ε-caprolactone) Diblock Copolymers. *Macromol. Symp.* **2004**, *215*, 369−382.
(53) Muller, A. J.; Albuerne, J.; Marquez, L.; Raquez, J.-M.; Degee, P.; Dubois, P.; Hobbs, J.; Hamley, I. W. Self-nucleation and crystallization kinetics of double crystalline poly(p-dioxanone)-b-poly([varepsilon]-caprolactone) diblock copolymers. *Faraday Discuss.* **2005**, *128*, 231−252.
(54) Lorenzo, A. T.; Arnal, M. L.; Sánchez, J. J.; Müller, A. J. Effect of annealing time on the self-nucleation behavior of semicrystalline polymers. *J. Polym. Sci. B: Polym. Phys.* **2006**, *44*, 1738−1750.
(55) Müller, A. J.; Lorenzo, A. T.; Arnal, M. L.; de Fierro, A. B.; Abetz, V. Self-Nucleation Behavior of the Polyethylene Block as Function of the Confinement Degree in Polyethylene-Block-Polystyrene Diblock Copolymers. *Macromol. Symp.* **2006**, *240*, 114−122.
(56) Castillo, R. V. n.; Müller, A. J.; Lin, M.-C.; Chen, H.-L.; Jeng, U. S.; Hillmyer, M. A. Confined Crystallization and Morphology of Melt Segregated PLLA-b-PE and PLDA-b-PE Diblock Copolymers. *Macromolecules* **2008**, *41*, 6154−6164.
(57) Loo, Y.-L.; Register, R. A.; Ryan, A. J.; Dee, G. T. Polymer Crystallization Confined in One, Two, or Three Dimensions. *Macromolecules* **2001**, *34*, 8968−8977.
(58) Castillo, R. V.; Arnal, M. L.; Muller, A. J.; Hamley, I. W.; Castelletto, V.; Schmalz, H.; Abetz, V. Fractionated Crystallization and Fractionated Melting of Confined PEO Microdomains in PB-b-PEO and PE-b-PEO Diblock Copolymers. *Macromolecules* **2008**, *41*, 879−889.
(59) Turnbull, D.; Fisher, J. C. Rate of Nucleation in Condensed Systems. *J. Chem. Phys.* **1949**, *17*, 71−73.
(60) Arnal, M. L.; López-Carrasquero, F.; Laredo, E.; Müller, A. J. Coincident or sequential crystallization of PCL and PEO blocks within polystyrene-b-poly(ethylene oxide)-b-poly(ε-caprolactone) linear triblock copolymers. *Eur. Polym. J.* **2004**, *40*, 1461−1476.
(61) Müller, A. J.; Balsamo, V.; Arnal, M. L.; Jakob, T.; Schmalz, H.; Abetz, V. Homogeneous Nucleation and Fractionated Crystallization in Block Copolymers. *Macromolecules* **2002**, *35*, 3048−3058.